HHS Public Access

Author manuscript

Nat Methods. Author manuscript; available in PMC 2019 August 25.

Published in final edited form as:

Nat Methods. 2019 March ; 16(3): 247–254. doi:10.1038/s41592-019-0329-7.

One-step generation of modular CAR-T with AAV-Cpf1

Xiaoyun Dai[*,1,2,3], **Jonathan J. Park**[*,1,2,3,4], **Yaying Du**[1,2,3], **Hyunu R. Kim**[1,2,3], **Guangchuan Wang**[1,2,3], **Youssef Errami**[1,2,3], and **Sidi Chen**[1,2,3,4,5,6,7,#]

[1]System Biology Institute, Yale University, West Haven, Connecticut, USA

[2]Department of Genetics, Yale University School of Medicine, New Haven, Connecticut, USA

[3]Center for Cancer Systems Biology, Integrated Science & Technology Center, Yale University, West Haven, Connecticut, USA

[4]Yale M.D.-Ph.D. Program, Yale University, New Haven, Connecticut, USA

[5]Immunobiology Program, Yale University, New Haven, Connecticut, USA

[6]Yale Comprehensive Cancer Center, Yale University, New Haven, Connecticut, USA

[7]Yale Stem Cell Center, Yale University, New Haven, Connecticut, USA

Abstract

Enhancing production efficiency, stability, effector function, and other desired features is of prime interest for chimeric antigen receptor engineered T cells (CAR-Ts). Here, we developed a new system for efficient generation of CAR-T with significantly enhanced features by streamlined genome engineering. Leveraging tracrRNA-independent CRISPR/Cpf1 systems with adeno-associated virus (AAV), building a stable CAR-T with homology-directed repair (HDR) knockin and checkpoint knockout (KIKO CAR-T) was achieved at high efficiency in one step. The modularity of the AAV-Cpf1 KIKO system enables flexible and highly efficient generation of double knockin of two different CARs in the same T cell. Compared to Cas9-based methods, the AAV-Cpf1 system generates double knockin CAR-Ts more efficiently. Dual-targeting CD22-specific AAV-Cpf1 KIKO CAR-T cells have potency comparable to Cas9 CAR-Ts in cytokine production and cancer cell killing, while expressing lower levels of exhaustion markers. This versatile system opens new capabilities of T cell immune engineering with simplicity and precision.

Introduction

Genome engineering in human primary T cells holds promise for the development of novel immunotherapeutics [1–5]. Genetically modified T cells expressing chimeric antigen receptors

[#] Correspondence: SC (sidi.chen@yale.edu), +1-203-737-3825 (office), +1-203-737-4952 (lab).
[*]These authors contributed equally to this work (co-first authors)

Author contributions

SC conceived the project. XD and SC designed the project. XD performed most experiments with the assistance of YD, RK, GW and YE. JJP developed computational pipelines and performed NGS data analysis. XD, JJP, and SC prepared the manuscript. SC secured funding and supervised the work.

(CARs) have recently been approved for the treatment of B-cell lymphoma and leukemia [6–8]. Currently approved CAR-T transgene delivery is based on randomly integrating lentiviral and γ-retroviral vectors, which carries the risk of insertional oncogenesis and translational silencing [9, 10]. Targeted integration of CD19 CAR into the *T cell receptor α constant (TRAC)* locus by CRISPR/Cas9 showed higher efficacy in a mouse model of acute lymphoblastic leukemia compared to conventionally generated CAR-Ts [11]. Recent methods to modify human T cells is based on Cas9 ribonucleoproteins (RNPs) [12], which can be combined with viral or non-viral templates [13, 14]. CRISPR/Cas9 systems also enable editing of endogenous loci to minimize T cell receptor (TCR) or human leukocyte antigen mediated graft-versus-host reactions (GVHR) [15, 16]. Clinical studies are on-going to test the effects of *Programmed Cell Death 1 (PDCD1/PD-1)* gene knockout in CAR-T cells for multiple myeloma or solid tumors (e.g. NCT03399448, NCT03545815). Although multiplex gene editing in CAR-T is possible with Cas9, it requires lentivirus transduction followed by electroporation of multiple components including Cas9 protein, guide RNAs produced *in vitro*, and homology-directed repair (HDR) template [15, 16], which complicates the manufacturing process. Better approaches to streamline multi-loci genome editing and achieve improved effector CAR-T function are of vital importance for human cell therapies.

Cas12a/Cpf1, a class 2 type V CRISPR system, is a multi-potent effector that can process crRNA arrays by itself and mediate DNA cleavage at multiple targets using a single customized CRISPR array [17–19]. In contrast to Cas9, Cpf1 is tracrRNA-independent and requires only a CRISPR RNA (crRNA) that consists of a 20~23 nt protospacer and a direct repeat (DR) [17–19]. Compared to Cas9, Cpf1 has higher specificity in human cells potentially due to its biochemical characteristics, and generates sticky-end double-stranded breaks (DSBs) that are less prone to non-homologous end joining (NHEJ), thus being ideal for precise gene editing [17–19]. Given these advantages, we set out to develop a platform for precise targeting of multiple loci in human primary T cells based on Cpf1. Using a combination of mRNA electroporation for LbCpf1 (Cpf1 from *Lachnospiraceae*) together with AAV6 for delivery of crRNA and HDR template (the combined system hereafter referred to as AAV-Cpf1), we achieved simple yet highly efficient targeting of both HDR-mediated dual-CAR knockin and immune checkpoint gene knockout (KIKO for short) in primary human T cells. KIKO CAR-T generated by the AAV-Cpf1 platform has multiple advantageous features such as CAR retention, cancer cell killing, effector function and resistance to exhaustion. This enables highly efficient generation of advanced CAR-T to streamline the creation of more complex genetically engineered T cells by modular processing.

Results

High-efficiency multiplexed genome editing with AAV-Cpf1 in human primary T cells

We optimized a workflow using AAV-Cpf1 for human primary T cell engineering (Fig. 1a). We delivered into human $CD4^+$ T cells a pseudouridine-modified LbCpf1 mRNA with 5' cap and poly A tail [20], and confirmed the expression of LbCpf1 protein that peaked on day one post-electroporation and diminishes on day four (Supplementary Fig. S1a). Using an AAV vector carrying a U6-promoter-driven Cpf1 crRNA targeting the 5′ end of the first

exon of *TRAC* (crTRAC) (Supplementary Fig. S1b), we titrated the targeting efficiency of AAV-Cpf1 with two AAV serotypes (AAV9 and AAV6) for packaging. Fluorescence activated cell sorting (FACS) analysis on TCR showed that both AAV9 and AAV6 carrying crTRAC reduced TCR^+ T cells in a multiplicity of infection (MOI)-dependent manner, with higher efficiency by AAV6 (Fig. 1b-c, Supplementary Fig. S1c). With Illumina Nextera amplicon library prep, next-generation sequencing (NGS) analysis showed on-target mutagenesis at the DNA level as evident by insertions and deletions (indels), which is also MOI-dependent (Supplementary Fig. S1d). We constructed an AAV vector carrying a crRNA array targeting both *TRAC* and *PDCD1* loci (crTRAC;crPDCD1), and showed that one transduction simultaneously generates editing in both loci using either AAV9 or AAV6, with the latter having high efficiency (Supplementary Fig. S2a-d). With AAV6-crTRAC;crPDCD1, NGS quantification showed that mutation efficiencies at *TRAC* and *PDCD1* loci in bulk unsorted cells reached 60.39% and 80.07%, respectively (Fig. 1d), which was further enriched by FACS sorting on the TCR^- population (78.80% and 83.63%, respectively) (Fig. 1d). These data demonstrated that AAV6 delivery of crRNA array with LbCpf1 mRNA electroporation is an efficient means for multiplexed editing in human primary T cells.

Modular and simultaneous knockin and knockout with AAV-Cpf1 in human primary T cells

We then leveraged the AAV vector to simultaneously deliver HDR template and crRNA array. We first tested knocking in a reporter gene dTomato into *TRAC* with simultaneous *PDCD1* knockout, using a single AAV construct $PDCD1^{KO}$;*dTomato-TRAC*^{KI} (*TRAC*-KIKO for short) (Fig. 2a, Supplementary Fig. S3a). Five days after electroporation and transduction, *TRAC*-KIKO mediated efficient, targeted dTomato integration as measured by flow cytometry (Fig. 2a). By staining CD3 that forms a surface complex with TCR [21], we detected TRAC:CD3 knockdown efficiency at >70%, with on-target integration of dTomato at >40% of total $CD4^+$ T cells (Fig. 2a, Supplementary Fig. S4a). We used a semi-quantitative In-Out PCR and confirmed *dTomato-TRAC* integration at the DNA level, with bulk HDR efficiency at 34.7% in unsorted cells and enriched to 69.5% in $CD3^-dTomato^+$ sorted cells by gel quantification (Supplementary Fig. S3b). NGS revealed the HDR junctions (Supplementary Fig. S3c), and also quantified the *dTomato-TRAC* HDR at 42.18% and 72.84% in bulk and enriched, respectively, with simultaneous measurements of *TRAC* wildtype and NHEJ alleles (Supplementary Fig. S3d). In the same samples, *PDCD1* knockout as indels at the predicted cleavage sites were also observed at bulk frequencies of 47% and 72% by T7E1 (NGS 62.34% and 87.03%) in unsorted and $TCR^-dTomato^+$ sorted cells (Supplementary Fig. S3e-f). The T7E1 result is likely an underestimate due to potential homoduplex mutants especially at high frequency [22]. To test knockin at sites other than *TRAC*, we generated another KIKO vector, $TRAC^{KO}$;*GFP-PDCD1*^{KI} (*PDCD1*-KIKO for short), to knockin a GFP reporter into the *PDCD1* locus while knocking out *TRAC* (Fig. 2b). Similarly, AAV-Cpf1 *PDCD1*-KIKO achieved >80% TCR knockdown with stable GFP integration in near 30% of treated $CD4^+$ T cells (Fig. 2b, Supplementary Fig. S4b).

The capacity to generate double knockin in the same T cell is essential for multi-feature CAR-T such as bi-specifics or multiple functional modulators. We then generated a dual-knockin AAV vector *dTomato-TRAC*^{KI};*GFP-PDCD1*^{KI} (TRAC-PDCD1-DKI for short),

where dTomato and GFP are targeted for integration into *TRAC* and *PDCD1* loci respectively. 5 days after electroporation and AAV6-TRAC-PDCD1-DKI transduction, 7.54% double positive GFP$^+$dTomato$^+$ T cells was produced, along with 5.97% GFP and 6.82% dTomato single positives (Fig. 2c, Supplementary Fig. S4c). An alternative strategy with two different AAV vectors (*PDCD1^{KO};dTomato-TRAC^{KI}* and *TRAC^{KO};GFP-PDCD1^{KI}*) for dual-targeting produced on average 13.83% GFP$^+$dTomato$^+$, 17.23% GFP$^+$ and 16.17% dTomato$^+$ T cells (Fig. 2d, Supplementary Fig. S4d). All the T cells that underwent integration (including single and double positives, Q1, Q2 and Q3) almost completely lost TCR expression, and 65% of non-integration T cells (GFP$^-$dTomato$^-$, Q4) lost TCR expression, whereas vector-transduced T cells mostly retained intact TCR (Fig. 2e). These data demonstrated simple, efficient, and precise double knockin of transgenes in human T cells by AAV-Cpf1 with crRNA arrays and HDR donors.

One-step generation of *TRAC* knockin CD22-specific CAR T cells with *PDCD1* disruption

Integration of anti-CD19 CAR (CAR19) into *TRAC* can improve pre-clinical efficacy in leukemia, and specific knockouts can reduce T cell exhaustion [11, 23, 24]. CD22-CAR targeting B-cell precursor acute lymphoblastic leukemia (ALL) was safe and provided high response rates for pediatric patients who failed chemotherapy and/or CAR19 treatment [25, 26]. We generated a single AAV construct *PDCD1^{KO};CD22BBz-TRAC^{KI}* (CD22BBz KIKO, or CAR22, for short) for knocking in CAR22 into *TRAC* with *PDCD1* knockout (Fig. 3a). Similarly, we showed that AAV-Cpf1 with CD22BBz KIKO generated precisely targeted knockin and knockout with limited toxicity and high viability (Fig. 3b, Supplementary Fig. S5a-b). With stimulation, the electroporated T cells quickly expanded over the course of 26 days observed (Supplementary Fig. S5c). Specifically, 44.6% of these T cells express *CD22BBz* CAR (Fig. 3b, Supplementary Fig. S6a). Semi-quantitative In-Out PCR as well as NGS confirmed *CD22BBz* integration at the *TRAC* locus, where bulk HDR efficiency with single transduction reached 45.46% in unsorted cells and enriched to 81.88% in CD3$^-$CAR22$^+$ sorted cells (Fig. 3c, Supplementary Fig. S6b-c). NHEJ variants of *TRAC* also exist at 13.01% in bulk and 9.97% in sorted populations on average (Fig. 3c). Simultaneous *PDCD1* knockout was observed high efficiency at 59.73% in bulk and 90.39% in CD3$^-$CAR$^+$ sorted T cells on average (Fig. 3d, Supplementary Fig. S6d). Virtually no detectable on-target mutation was found in uninfected control, indicating a clean background. Interestingly, the fraction of CAR22$^+$ T cells steadily increases over time, starting at 38.73% on day 3 and ramping up to 74.13% on day 9 after stimulation with target cells (Fig. 3e, Supplementary Fig. S6e), likely due to negative selection of non-functional cells. These data demonstrate a simple and rapid method to generate targeted knockin CAR with simultaneous immune checkpoint knockout at high efficiency using the AAV-Cpf1 KIKO system in one-step.

Modular generation of CD19 and CD22 bi-specific CAR-T cells with double knockin and simultaneous *TRAC;PDCD1* dual-disruption

We then tested whether AAV-Cpf1 KIKO can efficiently generate more complex CAR-Ts with simple engineering steps. We first generated an AAV vector *TRAC^{KO};CD19BBz-PDCD1^{KI}* (CD19BBz-KIKO for short) to mediate CD19BBz transgene knockin into the *PDCD1* locus with *TRAC* knockout (Supplementary Fig. S7a). We found that one

transduction can generate CD19BBz-*PDCD1* knockin at a bulk efficiency of 37.83%, with efficient *TRAC* knockout (Supplementary Fig. S7b-c). We then jointly transduced primary $CD4^+$ T cells with both CD22BBz-KIKO and CD19BBz-KIKO vectors to generate bi-specific CAR-T cells (Supplementary Fig. S7d). Five days post electroporation and transduction, FACS analysis revealed that one transduction generated dual knockin of $CD22BBz^+$;$CD19BBz^+$ double positive CAR-T cells at a bulk efficiency of 21.70%, with $CD22BBz^+$ and $CD19BBz^+$ single positive cells at bulk efficiency of 22.53% and 7.27% respectively (Supplementary Fig. S7e-f). All T cells that underwent integration (Q1, Q2 and Q3) had near-complete TCR disruption (Supplementary Fig. S7g). These results demonstrated one-step modular generation of engineered T cells with CD19BBz and CD22BBz double-knockin and simultaneous *TRAC;PDCD1* dual-disruption.

Comparing AAV-Cpf1 KIKO to Cas9-mediated single and double knockin CAR-T generation

We then compared the AAV-Cpf1 KIKO platform to Cas9-mediated CAR-T generation by targeting same CAR transgenes into the same loci. We first used Cas9 RNP with annealed crRNA and tracrRNA for electroporation to introduce double-stranded breaks, then infected with AAVs carrying CAR HDR templates. This generated knockin for CD22BBz CAR into the *TRAC* locus (CAR22), with an average of 44.40% $CAR22^+$ T cells on days 5 (Supplementary Fig. S8a-b). This result was confirmed with two independent *PDCD1* guide RNAs (Supplementary Fig. S8b). We also demonstrated CD19BBz CAR-T knockin into the *PDCD1* locus (CAR19) similarly (Supplementary Fig. S8c-d). We then performed double knockin using the Cas9 RNP electroporation followed by AAV infection with both CD22BBz and CD19BBz HDR templates. In parallel, we performed the AAV-Cpf1 KIKO pipeline, i.e. Cpf1 mRNA electroporation followed by infection of AAVs with crTRAC;crPDCD1 as well as CD22BBz and CD19BBz HDR templates. Interestingly, the AAV-Cpf1 KIKO double knockin pipeline efficiently generated $CAR19^+$;$CAR22^+$ double positive cells averaging 35.80% on day 8 (Fig. 4a, Supplementary Fig. S9a), whereas the Cas9 RNP double knockin pipeline only generated 3.20% (Fig. 4b, Supplementary Fig. S9b). Using different guide RNAs do not change the efficiency of $CAR19^+$;$CAR22^+$ double knockin for the Cas9 RNP system (Supplementary Fig. S9c). The frequency of $CAR19^+$;$CAR22^+$ double positive T cells generated by AAV-Cpf1 KIKO in the bulk unsorted population steadily increased from an average of 23.80% on day 5 to 61.73% on day 12 (Fig. 4c), and up to 76.33% on day 14–16 (Dataset S1). $CAR19^+$;$CAR22^+$ cells generated by the Cas9 RNP pipeline in the bulk unsorted population averaged at 2.56% on day 5 to 4.06% on day 12 (Fig. 4d). While Cpf1 and Cas9 represents two different nucleases and the two systems do not have strict parity, these data showed that, using current approaches, the AAV-Cpf1 KIKO platform is highly efficient for generating endogenous genomic loci targeted dual knockin CAR-Ts.

Immunological characteristics of single- and double- knockin CAR-Ts generated by AAV-Cpf1 KIKO system

We then compared the phenotypes of various CAR-T cells generated by the AAV-Cpf1 KIKO system. We utilized a cognate cancer cell line NALM6 ($CD19^+CD22^+$), and generated a NALM6-GL line that stably expressed GFP and luciferase (Supplementary Fig. S10a-c). We determined the cytolytic activity of CAR-T cells at different titration series of

effector:target (E:T) ratios in a co-culture setting (kill assay). Vector-transduced T cells have minimal cytolytic activity against NALM6-GL; in sharp contrast, all three forms of CAR-T cells generated by Cpf1 KIKO, i.e. CAR22, CAR19 and CAR22;CAR19 double knockins, have strong potency in killing NALM6-GL cancer cells in a dose-dependent manner (Supplementary Fig. S11a). These three forms of CAR-T cells have similar cytolytic activity (Supplementary Fig. S11a). We then measured the effector cytokine production and found that all three forms of CAR-Ts have highly boosted IFNγ and TNF-α production compared to vector-transduced T cells (Supplementary Fig. S11b-c). The CAR22;CAR19 double knockin CAR-T cells have relatively higher TNF-α and lower IFNγ productivity as compared to the single knockin counterparts (Supplementary Fig. S11b-c). These data demonstrated that both single and double knockin versions of AAV-Cpf1 KIKO generated CAR-T cells are robustly functional against cognate cancer cells.

Immunological characteristics of CD22BBz CAR-T generated by AAV-Cpf1 KIKO as compared to Cas9-mediated *TRAC* knockin and simultaneous *PDCD1* knockout

We then examined the immunological characteristics of the CAR-T cells generated by the AAV-Cpf1 KIKO platform in parallel with Cas9-mediated knockin and knockout (Fig. 5a). We found that the CD22BBz CAR-T generated by both AAV-Cpf1 KIKO (Cpf1 KIKO CD22BBz) and Cas9-mediated knockin and knockout (Cas9 RNP CD22BBz) are highly potent compared to vector-transduced T cells (Fig. 5b). Both Cpf1- and Cas9- generated CAR-T cells are potent IFNγ and TNF-α producers at comparable levels (Fig. 5c, Supplementary Fig. S12a). Interestingly, in contrast to Cas9 RNP CD22BBz, the Cpf1 KIKO CD22BBz CAR-T cells expressed lower levels of T cell exhaustion markers including PD-1, TIGIT and LAG3 (Fig. 5d, Supplementary Fig. S12b). These experiments demonstrated that the AAV-Cpf1 KIKO CAR targeting method generates engineered CAR-T cells with potent effector function and reduced levels of exhaustion with simpler transgene delivery, especially when involving the generation of double knockin CAR-Ts. Together with the production efficiency data above, these features suggest AAV-Cpf1 KIKO is a favorable system for rapid and efficient generation of multi-feature CAR-T cells with genomic precision and modular characteristics.

Discussion

As a “living drug”, genetically engineered CAR-T cells hold tremendous promise for potent and specific anti-tumor activity [6–8]. Currently, there are only two FDA-approved CAR-T platforms (Yescarta / axicabtagene ciloleucel, and Kymriah / tisagenlecleucel) for large B-cell lymphomas such as non-Hodgkin lymphoma (NHL) and B-cell ALL [4]. Most other leukemias and solid tumors do not have approved CAR-T therapy, although multiple pre-clinical and clinical studies are on-going with various forms of CAR-Ts [5]. Generation of CAR-T cells involves primary T cell isolation, transgene introduction, and expansion [27]. Transduction efficiency, transgene expression levels, and CAR stability or retention are all keys to this process. However, in lentiviral or retroviral transduction, CAR-T cells tend to lose their transgenes and therefore the ability to recognize and destroy cancer cells [28]. CRISPR/Cas9-mediated *TRAC* knockin improved CAR-T stability and function [11, 15]. The KIKO system utilizes AAV carrying both Cpf1 crRNA array for flexible multiplexed editing

and HDR constructs for introduction of CAR, holding significant advantages. This system is readily scalable to high-dimensional CAR-T engineering such as dual-targeting with two CARs and bi-specifics [26, 29], as well as introducing regulatory proteins such as auto-regulatory motifs, kill-switches, effector boosters, or dampeners [4].

The AAV-Cpf1 system combines both viral- and non-viral methods for CAR-T engineering. Delivery of the RNA-guided endonuclease (RGN) is mediated by transient expression of Cpf1 mRNA, and delivery of the crRNA and HDR template is mediated by stable AAV. This reduces potentially undesired continuous DSBs, while maintaining the need for stable presence of HDR template and crRNA to achieve higher knockin efficiency. Semi-comparative studies above showed that the AAV-Cpf1 KIKO method generates double knockins more efficiently than a current Cas9-based method. These CAR-T cells also express lower levels of exhaustion markers, which might be due to the higher efficiency of Cpf1 for generating multiple knockins and knockouts simultaneously. Of course, these two RGNs are fundamentally different in terms of biochemical mechanism. Given the high efficiency, rapid growth rate, auto-enriching characteristics of the AAV-Cpf1 KIKO CAR-T, we developed a standard set of procedures (Dai et al., *ProtocolExchange,* DOI: 10.1038/protex.2018.139) for generation of modular CAR-T cells. From the source of a regular blood draw, a total number of 300 million CAR-Ts (a typical number for clinical infusion) can be generated with a number of electroporation-AAV reactions following *in vitro* expansion for approximately two weeks (Dataset S1) [30]. While this study provides proof-of-concept for a new method that improves the early steps of CAR-T engineering, rigorous evaluation of toxicity profiles and *in vivo* efficacy testing need to be performed in the future prior to clinical applications. Given further optimization and *in vivo* testing, this platform, with its simplicity and modularity, has the potential to be broadly used as a research tool in T cell engineering, as well as a pipeline for improved “off-the-shelf” adoptive T cell therapies in the clinic.

Online Methods

Institutional Approval

This study has received institutional regulatory approval. All recombinant DNA and biosafety work was performed under the guidelines of Yale Environment, Health and Safety (EHS) Committee with an approved protocol (Chen-rDNA-15–45). All human sample work was performed under the guidelines of Yale University Institutional Review Board (IRB) with an approved protocol (HIC#2000020784).

T cell culture

Human primary peripheral blood $CD4^+$ T cells were acquired from healthy donors (STEMCELL Technologies). Cells were obtained using Institutional Review Board (IRB)-approved consent forms and protocols from the vendor (https://www.stemcell.com/human-peripheral-blood-cd4-t-cells-frozen.html). T cells were cultured in X-VIVO media (Lonza) with 5% human AB serum and recombinant human IL-2 30U/mL. Before electroporation, T cells were activated with 1:1 ratio of human anti-CD3/anti-CD28 beads (CD3/CD28

Dynabeads, ThermoFisher), which were later removed by magnetic separation rack after two days.

Generation of LbCpf1 mRNA

Human codon optimized LbCpf1 was from reference [19], which was then subcloned into a cDNA in vitro transcription vector. Pseudouridine-modified LbCpf1 mRNA with 5' cap and poly A tail was generated from the vector at TriLink.

Construction of AAV vectors

To generate an AAV crRNA expression vector (AAV-LbcrRNA, or pXD017), the U6-crRNA expression cassette with double BbsI cutting sites was synthesized and subcloned into an AAV backbone containing inverted terminal repeats (ITRs). The LbCpf1 crRNA was designed by Benchling to target the first exon of the *TRAC* locus and the second exon of *PDCD1* (Supplementary Table S1). Oligonucleotides (Yale Keck) with sticky ends were annealed, phosphorylated, and ligated into BbsI-digested vector by T4 ligase (NEB). To generate the HDR construct, the left and right homologous arms of the *TRAC* or *PDCD1* locus were amplified by PCR using locus-specific primer sets HDR-F1/R1 and HDR-F2/R2 from primary $CD4^+$ T cells. For transgene cloning, the HDR-R1 and HDR-F2 were connected with a multiple cloning site (MCS) (Supplementary Tables S1). Homologous donor templates were cloned into the AAV-LbcrRNA with or without a crRNA. CD22BBz CAR was generated as previously described [25]. Briefly, the CAR comprises a CD22 binding single chain variable fragment (scFV) m971 specific for the human CD22, followed by CD8 hinge-transmembrane-regions linked to 4–1BB (CD137) intracellular domains and CD3ζ intracellular domain. Based on a pXD017-dTomato backbone, m971-BBz was cloned into this vector using a gBlock (IDT). To generate CD19BBz CAR, the sequence of CD19 binding scFv (FMC63) was found from NCBI (GenBank: HM852952) and followed by CD8 hinge-transmembrane-regions linked to 4–1BB (CD137) intracellular domains and CD3ζ intracellular domain [31]. In order to detect CD19BBz CAR in different way, the Flag-tag sequence (GATTACAAAGACGATGACGATAAG) was added after CD8α leader sequence [32]. Based on a pXD017-dTomato backbone, FMC63-BBz was cloned into this vector using a gBlock (IDT). For making of HDR template, the EFS-dTomato-PA cassette, EFS-CAR22BBz-PA or EFS-CAR19BBz-PA cassette was cloned into the multi-clone site (MCS).

AAV production and titration

AAV was produced by transfecting HEK293FT cells (ThermoFisher) in 15-cm tissue culture dishes (Corning). Transfection was performed by using AAV2 transgene vectors, packaging (pDF6) plasmid, and AAV6/9 serotype plasmid together with polyethyleneimine (PEI). Transfected cells were collected using PBS after post-transfection 72 hours. For the AAV purification, transfected cells were mixed with pure chloroform (1/10 volume) and incubated at 37 °C with vigorously shaken for 1 h. NaCl was added to a final concentration of 1 M, and then the samples were centrifuged at 20,000g at 4 °C for 15 mins. The chloroform layer was discarded while the aqueous layer was transferred to another tube. PEG8000 was added to 10% (w/v) and shaken until dissolved. The mixture was incubated at 4 °C for 1 h and then centrifuged at 20,000g at 4 °C for 15 mins. The supernatant was discarded and the pellet was

suspended in DPBS with $MgCl_2$, treated with universal nuclease (ThermoFisher), and incubated at 37 °C for 30 mins. Chloroform (1:1 volume) was then added, shaken, and centrifuged at 12,000g at 4°C for 15 mins. The aqueous layer was isolated and concentrated through a 100-kDa MWCO (Millipore). Virus was titered by qPCR using custom Taqman assays (ThermoFisher) targeted to promoter U6.

T cell electroporation

Electroporation was performed after T cells were activated for 2 days. After using a magnetic holder to remove CD3/CD28 Dynabeads, cells were prepared at a density of 2×10^5 cells per 10 μL tip reaction or 2×10^6 cells per 100 μL tip reaction in electroporation Buffer R (Neon Transfection System Kits). T cells were mixed with 1 μg or 10 μg of modified NLS-LbCpf1mRNA (TriLink) according to reaction volume and electric shocked at program 24 (1,600V, 10ms and three pulses). After electroporation, the cells were transferred into 1mL of pre-warmed X-VIVO media (without antibiotics) immediately. Indicated volumes of AAV at a defined multiplicity of infection (MOI, specified in figure legends) were added into the T cells 2–4 hours after electroporation.

Cas9 RNP electroporation

RNPs were produced by complexing a two-component gRNA to Cas9, as previously described [13]. In brief, Cas9 guide RNA was designed to target the same sites as Cpf1 crRNA for *TRAC* and *PDCD1* using Benchling (Supplemental Table S1). Cas9 crRNAs and tracrRNAs were chemically synthesized (Dharmacon or IDT), and resuspended in nuclease-free IDTE buffer at a concentration of 160 μM. The crRNA and tracrRNA were mixed at 1:1 ratio and annealed as a guide RNA in Nuclease-Free IDTE buffer at 95°C for 5 min and 37°C for 10 min. Each guide was annealed separately and mixed as appropriate. RNPs were formed by the addition of SpCas9 nuclease (Dharmacon, IDT) with the 80 μM gRNA (1:2 Cas9 to sgRNA molar ratio) at benchtop for 15 min. RNPs were electroporated immediately after complexing. After 2~4 hours, AAV6 was added into cells at MOI = 1e5.

Generation of stable cell lines

Lentivirus including GFP-luciferase reporter genes were produced as previous described [33]. NALM6 cells (ATCC) were infected with 2x concentrated lentivirus by spinoculation in retronectin-coated (Takara) plates at 800g for 45 mins at 32°C. After infection for 2 days, the GFP-positive cells (NALM6-GL) were sorted on a BD FACSAria II. The second round sorting was performed after culture for two additional days. To test the luciferase expression in NALM6-GL, cells were incubated with 150μg/ml D-Luciferin (PerkinElmer) and bioluminescence signal intensity was measured by an IVIS system.

Flow cytometry

Surface protein expression was determined by flow cytometry. After electroporation for 5 days, 1×10^6 cells were incubated with APC-CD4, PE/Cy7-TCR (or PE-TCR) and FITC-CD3 antibodies (Biolegend) for 30 mins. For the CD22BBz CAR transduced T cells were incubated with 0.2 μg CD22-Fc (R&D system) in 100 μL PBS for 30 mins, and then stained with PE-IgG-Fc (Biolegend). For the CD19BBz CAR detection, the transduced T cells were

stained with APC-anti-DYKDDDDK Tag (Biolegend). Stained cells were measured and sorted on BD FACSAria II. For the T cell exhaustion assay, T cells from various groups were co-cultured with NALM6 cells at 0.5:1 E:T ratio for 24 hours. 1×10^6 cells were incubated with 0.2 μg CD22-Fc (R&D Systems) in 100 μL PBS for 30 mins and then stained with PE-IgG-Fc, PD-1-FITC, TIGIT-APC and LAG3-Percp/cy5.5 (Biolegend) for 30 mins. After washing twice, the stained cells were measured and sorted on BD FACSAria II, and analyzed using FlowJo software version 9.9.4 or 10.3 (Treestar, Ashland, OR).

Intracellular staining of IFNγ and TNF-α

Intracellular staining was performed to detect the expression level of IFNγ and TNF-α. After infection for 4 days, AAV-transduced CD22BBz CAR were co-cultured with NALM6 in fresh media which was supplied with brefeldin A and 2 ng/mL IL-2. After being incubated for 5 hours, T cells were collected and stained for surface CAR. After membrane protein staining, cells were fixed and permeabilized by fixation/permeabilization solution (BD), followed by addition of anti-IFNγ-APC or anti-TNF-α-FITC for intracellular staining. After 30 mins, the stained cells were washed by BD Perm/Wash™ buffer and measured by BD FACSAria II.

T cell : cancer cell co-culture (kill assay)

2×10^4 NALM6-GL cells were seeded in a 96 well plate. The modified or control T cells were co-cultured with NALM6-GL at indicated E:T ratios for 24 hours. Cell proliferation was tested by adding 150μg/ml D-Luciferin (PerkinElmer) into each well. After 5 mins, luciferase assay intensity was measured by a plate reader (PerkinElmer).

Analysis of HDR by In-Out PCR

A semi-quantitative In-Out PCR was performed as previously described to measure the rates of dTomato or CAR22 m971-BBz integration at the *TRAC* locus [34]. The assay used three primers in one PCR reaction. One primer recognizes a sequence contained in the dTomato or m971-BBz cassette; a second primer binds to genomic sequence outside of this AAV donor; the third primer binds to a sequence of the left *TRAC* homology arm (Supplementary Table S1). This PCR product, designated *TRAC*-HDR, was normalized by comparison to the product resulting from the control with genomic DNA isolated from normal human $CD4^+$ T cells.

Western blot analysis

Cells were lysed by ice-cold RIPA buffer (Boston BioProducts) containing protease inhibitors (Roche, Sigma) and incubated on ice for 30 mins. Protein supernatant was collected after centrifuging at 13,000g 4 °C for 30 mins. Protein concentration was determined using the Bradford protein assay (Bio-Rad). Protein samples were separated under reducing conditions on 4–15% Tris-HCl gels (Bio-Rad) and analyzed by western blotting using primary antibodies: mouse anti-LbCpf1 (Diagenode 1:3000) followed by secondary anti-rabbit HRP antibodies (Sigma-Aldrich, 1:10,000). Blots were imaged with an Amersham Imager 600.

Amplicon sequencing

The resultant PCR products were used for Nextera library preparation following the manufacturer's protocols (Illumina). Briefly, 1 ng of purified PCR product was fragmented and tagged using the Nextera Amplicon Tagment Mix according the to manufacturer's recommendations, followed by limited-cycle PCR with indexing primers and Illumina adaptors. After this amplification, DNA bands were purified with a gel extraction kit (Qiagen). Libraries were sequenced using 100-bp paired-end reads on an Illumina HiSeq 4000 instrument or equivalent, in general generating between 29 to 74 million reads per library. For indel quantification, paired reads were mapped to the amplicon sequences using BWA-MEM with the -M option. 100bp reads from the SAM file that fully mapped within a +/− 75bp window of expected cut site within the amplicon were then identified (soft-clipped reads discarded). Indel reads were then identified by the presence of "I" or "D" characters within the CIGAR string. Cutting efficiency was quantified as percentage of indels over total (indel plus wild-type) reads within the defined window. Indel variant statistics are provided in Supplementary Dataset S1, and the raw sequencing files are available via SRA.

HDR Mapping

For HDR quantification, FASTQ reads were mapped to possible amplicons based on primer combinations and HDR status. Mapping was performed for full amplicons and for "informative" amplicons, which were truncated so that 100bp reads would have at least 20bp homology with the CAR sequence (or with the other *TRAC* arm, in the case of wild-type sequences). Informative reads would be used to distinguish wild-type, NHEJ, and HDR reads with higher confidence. Paired reads were mapped to amplicon sequences using BWA-MEM with -M flag to generate SAM files. SAMtools was used to convert files to BAM, sort, index, and generate summary statistics of read counts with the idxstats option. To quantify wild-type vs NHEJ reads, take reads that mapped to "info_nonHDR" sequence (described below), and call reads with indels (I" or "D" characters within the CIGAR string) as NHEJ. Otherwise call reads as wild-type. Read counts were then pooled for downstream analysis. Description of amplicon sequences below:

amplicon_nonHDR: refers to full amplicon from F1 and R1 of genomic, wild-type DNA.

amplicon_CAR_F1: refers to full amplicon from F1 and R1 of expected, integrated CAR.

amplicon_CAR_F2: refers to full amplicon from F2 (primer site within the CAR as opposed to outside) and R1 of expected, integrated CAR.

info_nonHDR: same as amplicon_nonHDR, except truncated to 80bp of the *TRAC* arms.

info_CAR_F1: same as amplicon_CAR_F1, except truncated to 80bp of the *TRAC* arms flanking the *TRAC*-CAR interface.

info_CAR_F2: same as amplicon_CAR_F2, except truncated to 80bp of the *TRAC* arms flanking the *TRAC*-CAR interface (relevant to the right arm only, since F2 is within the CAR sequence).

HDR, NHEJ, and WT scores were calculated as follows:

info_nonHDR = info_WT + info_NHEJ

hdr_score = info_CAR_F2/(info_CAR_F2+info_nonHDR)

wt_score = info_WT/(info_CAR_F2+info_nonHDR)

nhej_score = info_NHEJ/(info_CAR_F2+info_nonHDR)

HDR statistics are provided in Supplementary Dataset S1, and the raw sequencing files are available via SRA.

Standard statistical analysis (non-NGS)

Standard data analysis (non-NGS) were performed using regular statistics, whereas NGS data were analyzed with specific pipelines described in Methods under separate sub-headlines. Data comparison between two groups was performed using a two-tailed unpaired *t*-test or non-parametric Wilcox test, where *p* values and statistical significance were estimated for all analyses. Data comparison between multiple groups with two factors was performed using a two-way ANOVA, where *p* values and statistical significance were estimated for all pairwise comparisons and adjusted for multiple testing. Prism (GraphPad Software Inc.) and RStudio were used for these analyses. All statistics are provided in Supplementary Dataset S1

Code availability

Analytic codes used to generate figures that support the findings of this study will be available from the corresponding author upon reasonable request.

Data and resource availability

Genome sequencing data are available via SRA with an accession number (PRJNA509600), pending data release in Jan 2019. Plasmids and libraries are being deposited to Addgene. A list of AAV vectors generated and used in this study is provided (Supplemental Table S2). Original and processed data are included in the figures, figure legends, and supplemental materials of this manuscript. Other relevant data and materials that support the findings of this study will be available from the corresponding author upon reasonable request.

Supplementary Material

Refer to Web version on PubMed Central for supplementary material.

Acknowledgments

We thank Drs. Charles Fuchs and Roy Herbst for their assistance and insightful discussions. We thank L Ye, J Li, L Shen, M Dong, R Chow, Z Bai, X Zhang, and all other members in Chen laboratory for technical assistance and discussions. We thank various colleagues in Department of Genetics, Systems Biology Institute, Cancer Systems Biology Center, MCGD Program, Immunobiology Program, BBS Program, Cancer Center and Stem Cell Center at Yale for assistance and/or discussion. We thank the Center for Genome Analysis, Center for Molecular Discovery, Pathology Tissue Services, Histology Services, High Performance Computing Center, West Campus Analytical Chemistry Core and West Campus Imaging Core and Keck Biotechnology Resource Laboratory at Yale, for technical support.

S.C. is supported by Yale SBI/Genetics Startup Fund, Damon Runyon Dale Frey Award (DFS-13–15), Melanoma Research Alliance (412806, 16–003524), St-Baldrick's Foundation (426685), Breast Cancer Alliance, Cancer Research Institute (CLIP), AACR (499395, 17–20-01-CHEN), The Mary Kay Foundation (017–81), The V Foundation (V2017–022), Ludwig Family Foundation, DoD (W81XWH-17–1-0235), Sontag Foundation, and NIH/NCI (1DP2CA238295–01, 1R01CA231112–01, 1U54CA209992–8697, 5P50CA196530-A10805, 4P50CA121974-A08306). GW is supported by CRI Irvington and RJ Anderson Postdoctoral Fellowships. J.J.P. is supported by the Yale MSTP training grant from NIH (T32GM007205).

Competing Financial Interests Statement

This research is primarily supported by Yale SBI/Genetics Startup Fund and NIH/NCI. The funder has no role in the conceptualization, design, data collection, analysis, decision to publish, or preparation of the manuscript. A provisional patent has been filed by the corresponding author at Yale University related to this study.

References

1. Garfall AL et al. Chimeric Antigen Receptor T Cells against CD19 for Multiple Myeloma. N Engl J Med 373, 1040–1047 (2015). [PubMed: 26352815]
2. Tebas P et al. Gene editing of CCR5 in autologous CD4 T cells of persons infected with HIV. New England Journal of Medicine 370, 901–910 (2014). [PubMed: 24597865]
3. Jackson HJ, Rafiq S & Brentjens RJ Driving CAR T-cells forward. Nat Rev Clin Oncol 13, 370–383 (2016). [PubMed: 27000958]
4. Labanieh L, Majzner RG & Mackall CL Programming CAR-T cells to kill cancer. Nature Biomedical Engineering 2, 377 (2018).
5. Rosenbaum L Tragedy, perseverance, and chance—the story of CAR-T therapy. New England Journal of Medicine 377, 1313–1315 (2017). [PubMed: 28902570]
6. Porter DL, Levine BL, Kalos M, Bagg A & June CH Chimeric antigen receptor–modified T cells in chronic lymphoid leukemia. New England Journal of Medicine 365, 725–733 (2011). [PubMed: 21830940]
7. Kalos M et al. T cells with chimeric antigen receptors have potent antitumor effects and can establish memory in patients with advanced leukemia. Science translational medicine 3, 95ra73–95ra73 (2011).
8. Neelapu SS et al. Axicabtagene Ciloleucel CAR T-Cell Therapy in Refractory Large B-Cell Lymphoma. N Engl J Med 377, 2531–2544 (2017). [PubMed: 29226797]
9. Themis M et al. Oncogenesis following delivery of a nonprimate lentiviral gene therapy vector to fetal and neonatal mice. Molecular Therapy 12, 763–771 (2005). [PubMed: 16084128]
10. Howe SJ et al. Insertional mutagenesis combined with acquired somatic mutations causes leukemogenesis following gene therapy of SCID-X1 patients. The Journal of clinical investigation 118 (2008).
11. Eyquem J et al. Targeting a CAR to the TRAC locus with CRISPR/Cas9 enhances tumour rejection. Nature 543, 113 (2017). [PubMed: 28225754]
12. Schumann K et al. Generation of knock-in primary human T cells using Cas9 ribonucleoproteins. Proceedings of the National Academy of Sciences 112, 10437–10442 (2015).
13. Roth TL et al. Reprogramming human T cell function and specificity with non-viral genome targeting. Nature 559, 405 (2018). [PubMed: 29995861]
14. Bak RO, Dever DP & Porteus MH CRISPR/Cas9 genome editing in human hematopoietic stem cells. Nature protocols 13, 358 (2018). [PubMed: 29370156]
15. Ren J et al. A versatile system for rapid multiplex genome-edited CAR T cell generation. Oncotarget 8, 17002 (2017). [PubMed: 28199983]
16. Liu X et al. CRISPR-Cas9-mediated multiplex gene editing in CAR-T cells. Cell research 27, 154 (2017). [PubMed: 27910851]
17. Zetsche B et al. Multiplex gene editing by CRISPR–Cpf1 using a single crRNA array. Nature biotechnology 35, 31 (2017).
18. Kleinstiver BP et al. Genome-wide specificities of CRISPR-Cas Cpf1 nucleases in human cells. Nature biotechnology 34, 869 (2016).

19. Zetsche B et al. Cpf1 is a single RNA-guided endonuclease of a class 2 CRISPR-Cas system. Cell 163, 759–771 (2015). [PubMed: 26422227]
20. Li B et al. Engineering CRISPR-Cpf1 crRNAs and mRNAs to maximize genome editing efficiency. Nat Biomed Eng 1 (2017).
21. Torikai H et al. A foundation for" universal" T-cell based immunotherapy: T-cells engineered to express a CD19-specific chimeric-antigen-receptor and eliminate expression of endogenous TCR. Blood, blood-2012–2001-405365 (2012).
22. Kim H et al. Surrogate reporters for enrichment of cells with nuclease-induced mutations. Nature methods 8, 941 (2011). [PubMed: 21983922]
23. Rafiq S et al. Targeted delivery of a PD-1-blocking scFv by CAR-T cells enhances anti-tumor efficacy in vivo. Nature biotechnology (2018).
24. Ren J et al. Multiplex genome editing to generate universal CAR T cells resistant to PD1 inhibition. Clinical cancer research (2016).
25. Haso W et al. Anti-CD22-chimeric antigen receptors targeting B cell precursor acute lymphoblastic leukemia. Blood, blood-2012–2006-438002 (2012).
26. Fry TJ et al. CD22-targeted CAR T cells induce remission in B-ALL that is naive or resistant to CD19-targeted CAR immunotherapy. Nature medicine 24, 20 (2018).
27. Levine BL, Miskin J, Wonnacott K & Keir C Global manufacturing of CAR T cell therapy. Molecular Therapy-Methods & Clinical Development 4, 92–101 (2017). [PubMed: 28344995]
28. Ellis J Silencing and variegation of gammaretrovirus and lentivirus vectors. Human gene therapy 16, 1241–1246 (2005). [PubMed: 16259557]
29. Majzner RG & Mackall CL Tumor Antigen Escape from CAR T-cell Therapy. Cancer discovery (2018).
30. Maude SL et al. Chimeric antigen receptor T cells for sustained remissions in leukemia. New England Journal of Medicine 371, 1507–1517 (2014). [PubMed: 25317870]

Additional References

31. Zetsche B et al. Cpf1 is a single RNA-guided endonuclease of a class 2 CRISPR-Cas system. Cell 163, 759–771 (2015). [PubMed: 26422227]
32. Haso W et al. Anti-CD22-chimeric antigen receptors targeting B cell precursor acute lymphoblastic leukemia. Blood, blood-2012–2006-438002 (2012).
33. Kochenderfer JN et al. Construction and pre-clinical evaluation of an anti-CD19 chimeric antigen receptor. Journal of immunotherapy (Hagerstown, Md.: 1997) 32, 689 (2009).
34. Han C et al. Desensitized chimeric antigen receptor T cells selectively recognize target cells with enhanced antigen expression. Nature communications 9, 468 (2018).
35. Roth TL et al. Reprogramming human T cell function and specificity with non-viral genome targeting. Nature 559, 405 (2018). [PubMed: 29995861]
36. Chen S et al. Genome-wide CRISPR screen in a mouse model of tumor growth and metastasis. Cell 160, 1246–1260 (2015). [PubMed: 25748654]
37. Wang J et al. Highly efficient homology-driven genome editing in human T cells by combining zinc-finger nuclease mRNA and AAV6 donor delivery. Nucleic Acids Res 44, e30 (2016). [PubMed: 26527725]

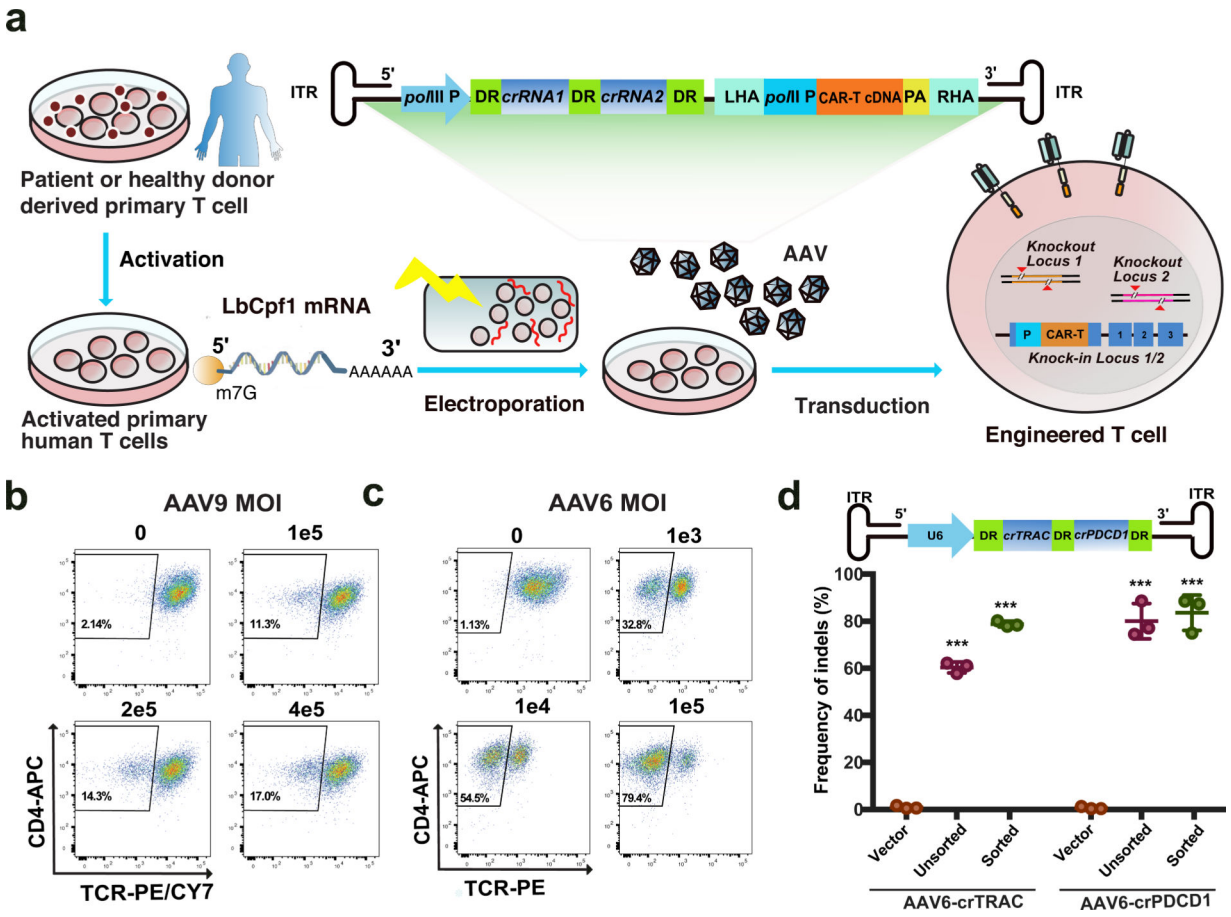

Figure 1. AAV-Cpf1 mediated efficient multiplexed genome editing in human primary CD4$^+$ T cells

(**a**) Schematic of LbCpf1 mRNA electroporation combined with AAV-delivered sgRNA and HDR template (AAV-Cpf1), enabling knockout and knockin of different genes in human primary T cells.

(**b-c**) Efficiency of AAV9 (**b**) and AAV6 (**c**) mediated TCR knockout on human primary CD4$^+$ T cells using FACS. One representative sample's data were shown from 1 to 5 biological replicates as indicated in (Supplementary Figure S01c).

(**d**) (Top) Schematic of a double-knockout AAV6-crRNA array targeting *PDCD1* and *TRAC*. (Bottom) Quantification of frequency of CRISPR/Cpf1 mediated double knockout of *PDCD1* and *TRAC* from human primary CD4$^+$ T cells after AAV6 infection for 5 days (n = 3 independent infection replicates). Unpaired two-sided t test was used for assess significance. Knockout vs. uninfected, *** $p < 0.001$ for all comparisons. Precise p values, up to the precision of 1e-15, are provided in Dataset S1, similarly thereafter. Data are shown as mean ± s.e.m., plus individual data points on the graph.

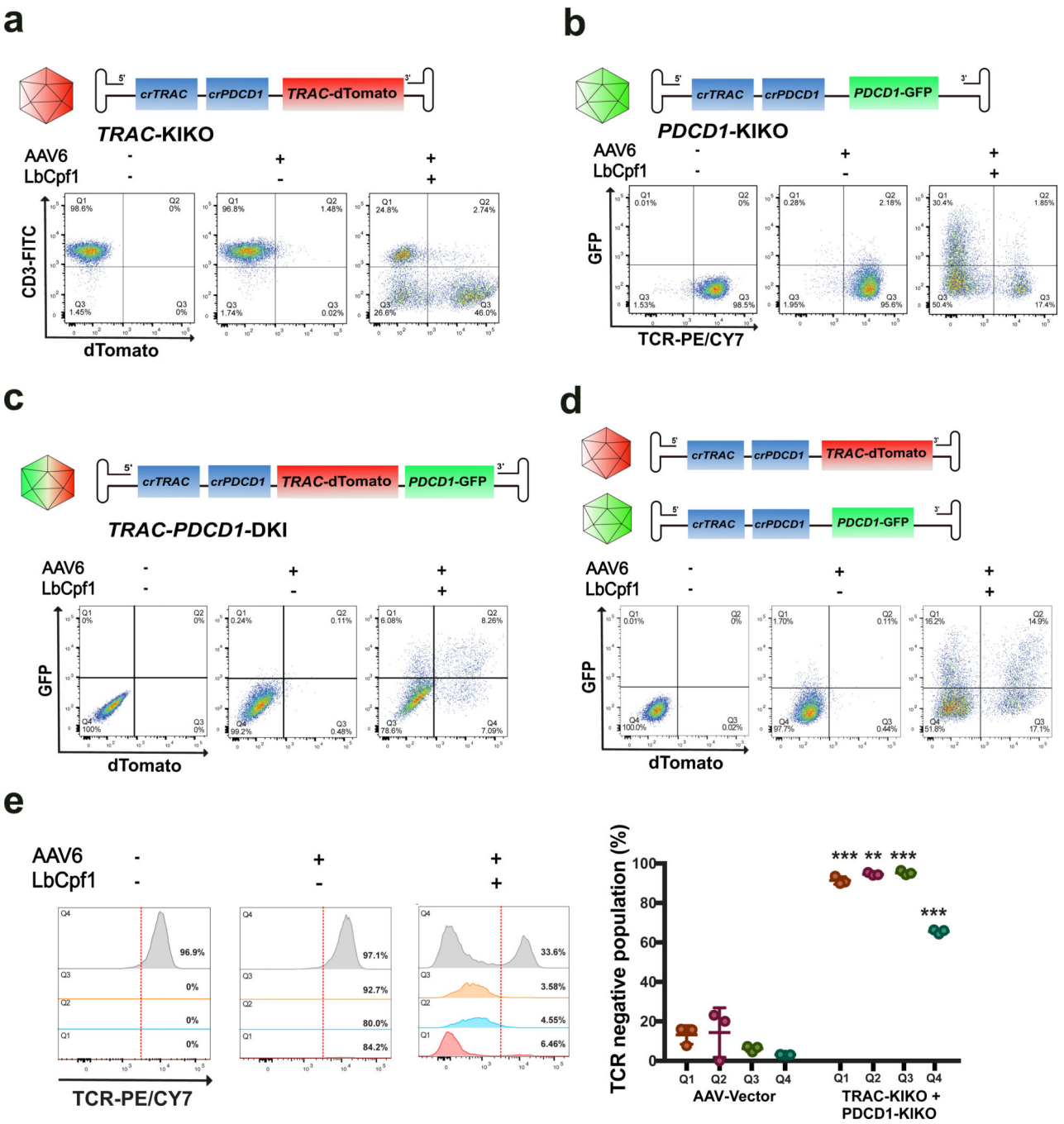

Figure 2. Modular combinations of AAV-Cpf1 mediated efficient multiplex knockin and knockout in human primary CD4^{+} T cells

(**a**) AAV-Cpf1 mediated dTomato transgene knockin into *TRAC* locus with *PDCD1* knockout. (Top) Schematics of construct design for *PDCD1*^{KO}*;dTomato-TRAC*^{KI} (*TRAC*-KIKO for short). (Bottom) Representative *TRAC* dTomato knockin flow cytometry plots were shown 5 days post AAV transduction (AAV6 packaging, MOI = 1e5). Experiments were done with 3 infection replicates, where quantifications and statistics are shown in Supplementary Figure S04a.

(**b**) AAV-Cpf1 mediated GFP transgene knockin into *PDCD1* locus with *TRAC* knockout. (Top) Schematics of construct design for $TRAC^{KO};GFP\text{-}PDCD1^{KI}$ (*PDCD1*-KIKO for short). (Bottom) Representative *PDCD1* GFP knockin flow cytometry plots were shown 5 days post AAV transduction (AAV6 packaging, MOI = 1e5). Experiments were done with 6 infection replicates, where quantifications and statistics are shown in Supplementary Figure S04b.

(**c**) AAV-Cpf1 mediated double knockin with a single vector. (Top) Schematics of construct design for a double knockin AAV vector $dTomato\text{-}TRAC^{KI};GFP\text{-}PDCD1^{KI}$ (TRAC-PDCD1-DKI for short), where dTomato and GFP are targeted to be integrated into *TRAC* locus and *PDCD1* locus respectively. (Bottom) Representative double knockin flow cytometry plots were shown 5 days post transduction of a single AAV construct (AAV6 packaging, MOI = 1e5). Experiments were done with 3–4 infection replicates, where quantifications and statistics are shown in Supplementary Figure S04c.

(d) AAV-Cpf1 mediated double knockin with a two-vector system. (Top) Schematics of construct design for using both $PDCD1^{KO};dTomato\text{-}TRAC^{KI}$ and $TRAC^{KO};GFP\text{-}PDCD1^{KI}$ for dual-targeting. (Bottom) Representative double knockin flow cytometry plots were shown 5 days post transduction of both AAV constructs (AAV6 packaging, MOI = 1e5). Experiments were done with 3 infection replicates, where quantifications and statistics are shown in Supplementary Figure S04d.

(**e**) Analysis of TCR knockout efficiency in knockin cells by FACS. (Left) Representative flow cytometry plots of the TCR expression levels in non-integration (Q4), single integration (Q1, Q3) or double integration (Q2) T cells from two-vector system. An example workflow of FACS gating plots are shown in Supplementary Figure S13. (Right) Quantification of TCR^- percentages in different quadrants shown in column graph (infection replicates, n = 3). Unpaired two-sided t test was used for assess significance. TCR^- population, Vector vs. dual-targeting, ** $p < 0.01$, *** $p < 0.001$. Data are shown as mean ± s.e.m.

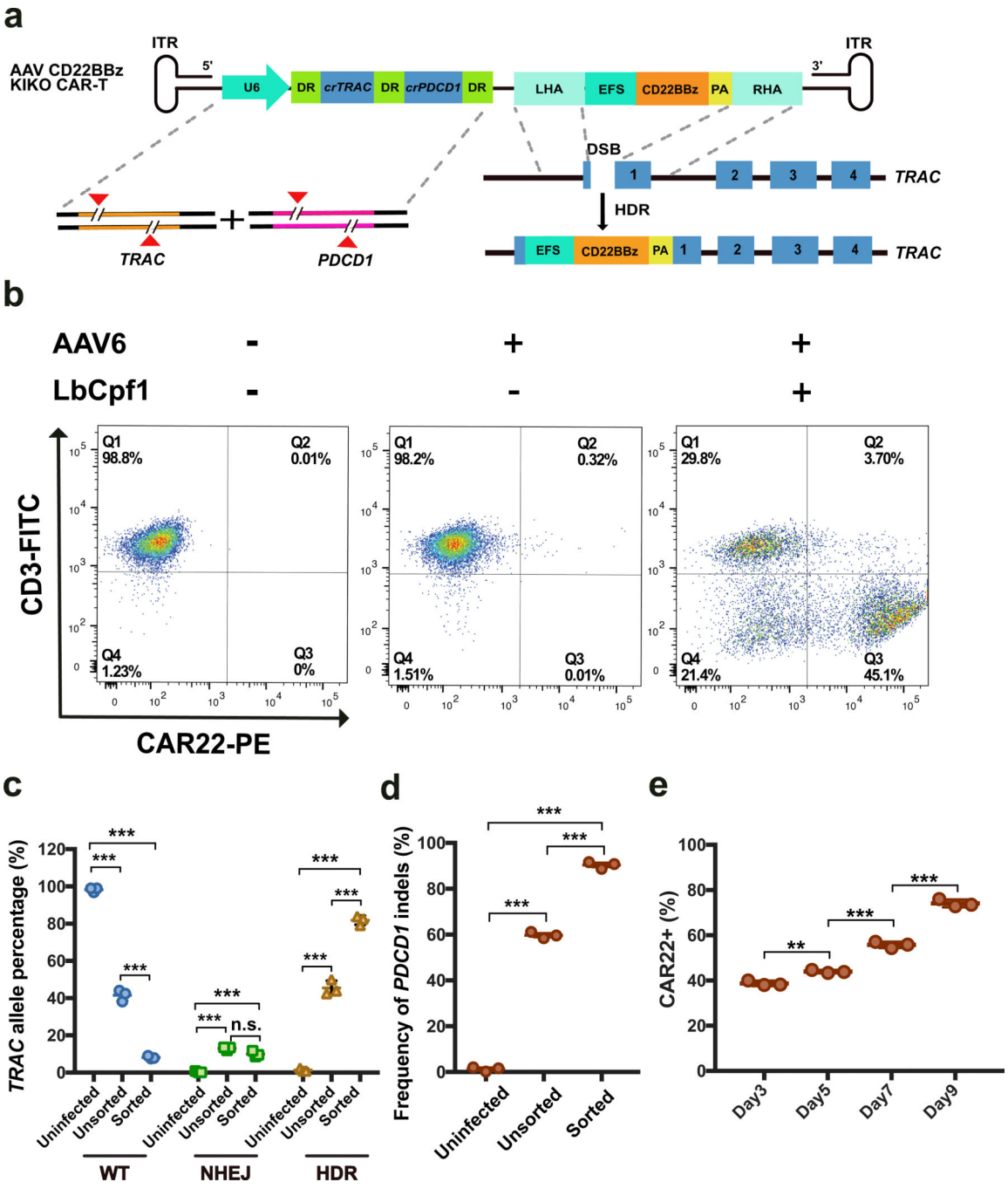

Figure 3. High-efficiency generation of stably integrated anti-CD22 CAR-T with *PDCD1* knockout by AAV-Cpf1 KIKO in one step

(**a**) Schematic of a single AAV construct *PDCD1*^{KO};*CD22BBz-TRAC*^{KI} (CD22BBz KIKO for short) for delivering a double-targeting crRNA array and an HDR template, mediating *CD22BBz* CAR integration into the *TRAC* locus with *PDCD1* knockout. The HDR template contains an EFS-*CD22BBz* CAR-PA cassette, where the *CD22BBz* CAR transgene is driven by an EFS promoter and terminated by a short polyA, flanked by two arms homologous to the *TRAC* locus. AAV Vector sample was only infected with AAV6 carrying the same construct, but did not receive electroporation of Cpf1 mRNA, thereafter.

(**b**) Representative flow cytometry plots of human primary $CD4^+$ T cells 5 days post AAV6 transduction (MOI = 1e5), showing the detection of *CD22BBz* transgene expression on T cell surface only with the AAV-Cpf1 targeting of $PDCD1^{KO}$;*CD22BBz-*$TRAC^{KI}$. Experiments were done with 3 infection replicates, where quantifications and statistics are shown in Supplementary Figure S06a.

(**c**) Quantitative allele mapping of *TRAC* locus for *CD22BBz* HDR, NHEJ, and wildtype (WT) reads with n = 3 infection replicates. Unpaired two-sided t test was used for assess significance.

WT group:

Vector vs. Unsorted, *** $p < 0.001$; Vector vs. Sorted, *** $p < 0.001$; Unsorted vs. Sorted, *** $p < 0.001$.

NHEJ group:

Vector vs. Unsorted, *** $p < 0.001$; Vector vs. Sorted, *** $p < 0.001$; Unsorted vs. Sorted, n.s..

HDR group:

Vector vs. Unsorted, *** $p < 0.001$; Vector vs. Sorted, *** $p < 0.001$; Unsorted vs. Sorted, *** $p < 0.001$.

Data are shown as mean ± s.e.m..

(**d**) Quantitative analysis for genomic knockout of *PDCD1* by $PDCD1^{KO}$;*CD22BBz-*$TRAC^{KI}$ in human primary $CD4^+$ T cells. Unpaired two-sided t test was used for assess significance. Vector vs. Unsorted, *** $p < 0.001$; Vector vs. Sorted, *** $p < 0.001$; Unsorted vs. Sorted, *** $p < 0.001$. Data are shown as mean ± s.e.m., plus individual data points on the graph.

(**e**) Time-course analysis of CAR transgene retention after transduction. CAR22 expression levels of $PDCD1^{KO}$;*CD22BBz-*$TRAC^{KI}$ bulk targeted CAR-T cells were shown by dot plot (infection replicates, n = 3). The bulk T cells were stimulated once with mitomycin C-treated NALM6 cells ($CD22^+$, Supplemental Figures) 5 days post transduction. CAR expression was measured by staining with a specific antibody follow by flow cytometry. One-way ANOVA with Tukey's multiple comparisons test was used for assess significance. ** $p < 0.01$; *** $p < 0.001$. Data are shown as mean ± s.e.m., plus individual data points on the graph.

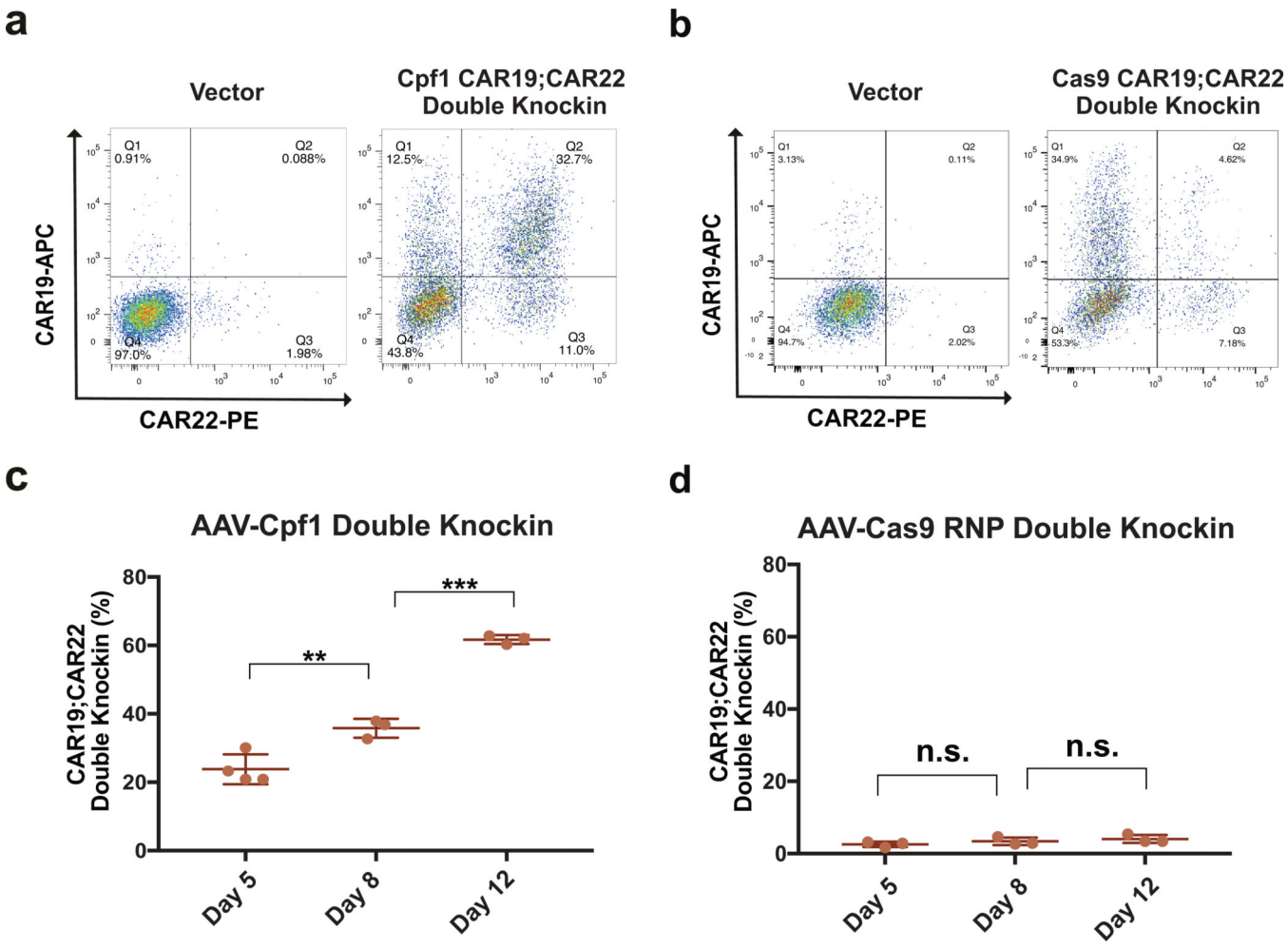

Figure 4. AAV-Cpf1 yield higher double CAR knockin than AAV-Cas9.

(**a**) Representative double knockin flow cytometry plots for AAV-Cpf1 mediated double knockin with a two-vector system (*PDCD1*^{KO}*;CD22BBz-TRAC*^{KI} + *TRAC*^{KO}*;CD19BBz-PDCD1*^{KI}), 8 days post transduction of both AAV constructs (AAV6 packaging, MOI = 1e5). Experiments were done with 3 infection replicates, where quantifications and statistics are shown in Supplementary Figure S09a.

(b) Representative double knockin flow cytometry plots for AAV-Cas9 RNP mediated double knockin with a two-vector system (two AAVs with CAR19 and CAR22 HDR templates targeting *PDCD1* and *TRAC* loci, respectively), 8 days post transduction of both AAV constructs (AAV6 packaging, MOI = 1e5). Experiments were done with 4–6 infection replicates, where quantifications and statistics are shown in Supplementary Figure S09b.

(c) Time-course analysis of double CAR transgene retention after transduction. CAR19 and CAR22 expression levels were shown by dot plot (infection replicates, day 5, n = 4; day 8 and day 12, n = 3). One-way ANOVA with Tukey's multiple comparisons test was used for assess significance. ** $p < 0.01$; *** $p < 0.001$.

(d) Time-course analysis of double CAR transgene retention after transduction. CAR19;CAR22 expression levels were shown by dot plot (infection replicates, n=3). n.s. not significant.

For both **(c)** and **(d):** Bulk T cells were stimulated once with target cells at 5 days post transduction. Data are shown as mean ± s.e.m., plus individual data points on the graph.

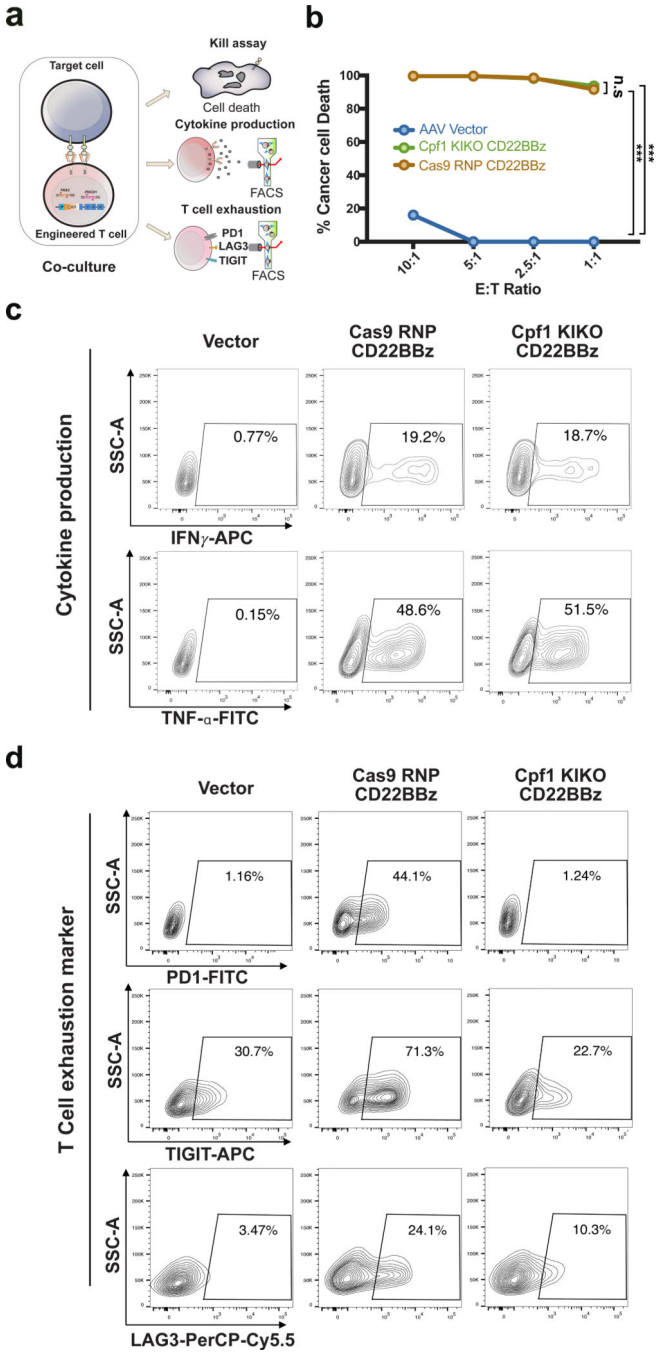

Figure 5. Cpf1 CD22BBz KIKO CAR-T outperforms to Cas9-mediated CD22BBz knockin and *PDCD1* knockout CAR-T.

(**a**) Pipeline for functional testing of Cpf1 CD22BBz KIKO CAR-T and Cas9 RNP CD22BBz CAR-T.

(**b**) Comparison of Cpf1 CD22BBz KIKO vs. Cas9 RNP CD22BBz CAR-T cells by kill assay. *In vitro* cytotoxic activity of CAR T cells on cancer cells was measured by bioluminescence assay at different effector:target (E:T) ratios, using NALM6-GL as target cells which have been stably transduced with GFP and luciferase genes (Supplemental

Figures). Cancer cell death % was shown for a titration series of E:T ratios for AAV Vector transduced T cells. Two-way ANOVA with Tukey's multiple comparisons test was used for assess significance (multiple-testing corrected). Cpf1 CD22BBz CAR vs. Vector, *** $p < 0.001$; Cas9 RNP CD22BBz CAR vs. Vector, *** $p < 0.001$; Cpf1 vs Cas9, n.s., not significant.

(**c**) Representative flow cytometry results showing that IFNγ and TNF-α expression levels in Cpf1 CD22BBz KIKO vs. Cas9 RNP CD22BBz CAR-T cells. IFNγ and TNF-α production was tested by intracellular staining after co-cultured with NALM6 for 5 hours at E:T= 1:1. Experiments were done with 3 infection replicates, where quantifications and statistics are shown in Supplementary Figure S12a.

(**d**) Representative flow cytometry results showing that T cell exhaustion marker expression level in Cpf1 CD22BBz KIKO vs. Cas9 RNP CD22BBz CAR-T cells. PD-1, TIGIT, and LAG3 expression was tested by surface staining after co-culture with NALM6 for 24 hours at E:T= 0.5:1. Experiments were done with 3 infection replicates, where quantifications and statistics are shown in Supplementary Figure S12b.

All data are shown as mean ± s.e.m., plus individual data points on the graph.